Towards Hyper-Reduction of Cardiac Models using Poly-Affine Deformation

Gaëtan Desrues, Hervé Delingette, Maxime Sermesant

Towards Hyper-Reduction of Cardiac Models using Poly-Affine Deformation

Gaëtan Desrues, Hervé Delingette, and Maxime Sermesant

Inria, University Côte d'Azur, Sophia Antipolis, France

Abstract. This paper presents a method for frame-based finite element model in order to develop fast personalised cardiac electromechanical models. Its originality comes from the choice of the deformation model: it relies on a reduced number of degrees of freedom represented by affine transformations located at arbitrary control nodes over a tetrahedral mesh. This is motivated by the fact that cardiac motion can be well represented by such poly-affine transformations. The shape functions use then a geodesic distance over arbitrary Voronoï-like regions containing the control nodes. The high order integration of elastic energy density over the domain is performed at arbitrary integration points. This integration, which is associated to affine degrees of freedom, allows a lower computational cost while preserving a good accuracy for simple geometry. The method is validated on a cube under simple compression and preliminary results on simplified cardiac geometries are presented, reducing by a factor 100 the number of degrees of freedom.

Keywords: Model Order Reduction · Finite Elements Method · Affine Transformation · Meshless.

1 Introduction

Patient specific cardiac modelling is important for understanding pathologies, planning a therapy or rehearsing a surgery. In order to be used in routine by clinicians, models have to be fast enough and provide an accurate solution to given boundary and initial conditions. The finite element method is a classical approach to solve physically based deformation problems where the computational domain depends on an underlying mesh, implying that the computation time and the accuracy will depend on the mesh discretization. Particle-based meshless frameworks have recently been proposed [2, 3] and have the advantage of being less dependent from the topology. Particles, called control nodes, can be placed arbitrarily. It has also been shown in the literature [5, 7] that cardiac motion can be well represented by mixing affine tranformations located at the center of sub-regions of the American Heart Association (AHA) segments, see Fig. 1. Furthermore, the decomposition into a mixture of affine transformations provides clinically interpretable parameters related to cardiac strain.

The key idea of this paper is to combine these approaches to propose an efficient reduced model. Compared to other reduced models using statistical

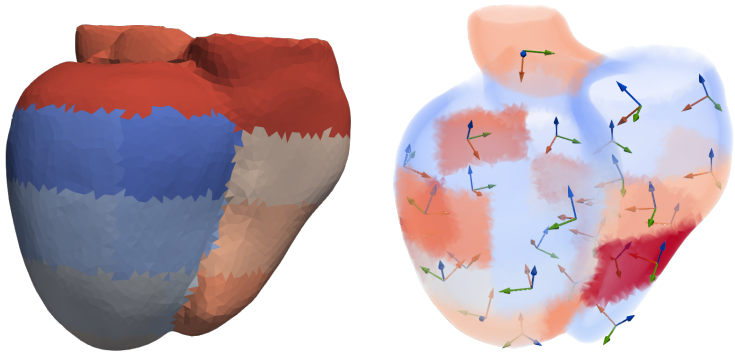

Fig. 1. 29 AHA regions (left) and oriented control nodes (right)

learning of a reduced basis, this approach builds upon physiological knowledge of the cardiac function to propose a novel reduction.

We first define the degrees of freedom (DOFs), regions and integration points. The internal forces resulting from the deformation of the solid are computed based on the minimization of an elastic energy density, itself resulting from the relation between strain and stress.

Fig. 2 presents the famework used in our simulation of elastic solids. The different elements and the link between them through mappings will be described in further sections.

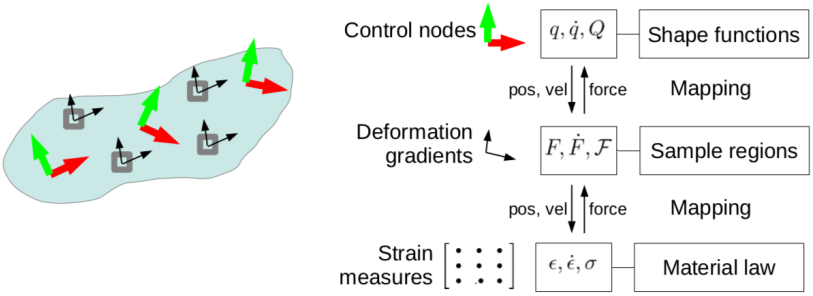

Fig. 2. Three levels continuum mechanics. The shape functions map the degrees of freedom, supported by the control nodes, to the deformation gradients located in the sample regions (grey square). Then, the material law computes the internal forces from the stress and strain. These forces are finally mapped back to the degrees of freedom. This process is repeated at each simulation step. Source: Flexible plugin documentation (Sofa-framework).

2 Frame-based deformation

Our scheme relies on a reduced number of affine frames as degrees of freedom acting on a tetrahedral mesh $\mathcal{V}$. If N is the number of vertices of $\mathcal{V}$, the classical approach is to define a displacement field based on the displacement of each vertex, which makes this field of dimension $3N$. Yet the cardiac motion usually does not require such high number of DOFs since the motion of neighboring vertices is highly correlated. This is why we propose to discretize the displacement field as a combination of n affine frame motions which makes it a $12n$ dimensional space. Instead of the 3-coordinate vector displacement field classically used, we propose to use a poly-affine displacement field for which at each control node $\mathbf{q}_i,\ 1 \leq i \leq n$, the 12 DOFs are the 12 coefficients of the affine transformation $\mathbf{T}(\mathbf{q}_i) = \mathbf{T}_i \in \mathcal{M}_{3\times 4}$ (3 coefficients for the 3D translation and 9 for the linear transformation combining rotation, scaling and shearing).

The whole computational domain Ω is partitioned into n non overlapping regions Ω_i, centered on $\mathbf{q}_i$, each region being defined as a set of tetrahedra.

At a point x in the domain, the local affine transformation $\mathbf{T}(x)$ is defined as a weighted sum of DOFs $\mathbf{T}_i$:

$$\forall x \in \Omega,\ \mathbf{T}(x) = \sum_{i=1}^{n} \phi_i(x)\mathbf{T}_i$$

The weights $\phi(x)$ are the shape functions and represent the influence of the control frames over the domain. Their definition depends on the mesh geodesic signed distance $\mathcal{D}_i(x)$ of a point x with respect to region i:

$$\forall x \in \Omega,\ \forall i \in [\![1, n]\!],\ \mathcal{D}_i(x) \begin{cases} = 0 & \text{on the border of } \Omega_i \\ < 0 & \text{inside } \Omega_i \\ > 0 & \text{outside } \Omega_i \end{cases}$$

This distance is computed after solving an Eikonal problem with fast marching method [6]. It is normalized as $\bar{\mathcal{D}}_i(x)$ such that its minimum value is -1 at its center $\mathbf{q}_i$.

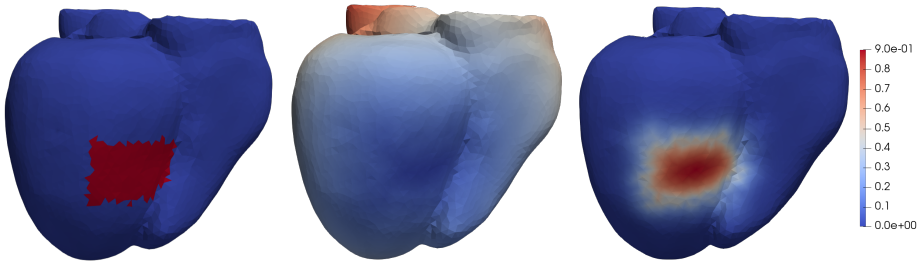

(a) Elements of the region (b) Geodesic distance (c) Shape function

Fig. 3. Example on a cardiac topology

If σ_a is the sigmoid function, the shape function ϕ_i is defined as:

$$\phi_i(x) = \sigma_a\left[\bar{\mathcal{D}}_i(x)\right], \quad \sigma_a(x) = \frac{1}{1+e^{ax}}$$

The parameter a controls the overlap of the kernel function over neighboring regions. We observed better results with $a = 2.25$, thus $\phi_i(\mathbf{q}_i) = 0.90$. It has been noticed that a big overlap (a small) leads to a smooth solution while a small one leads to more independent regions, in both cases introducing unrealistic values in the solution. An example with $a = 2.25$ is presented in Fig. 3(c).

3 Numerical integration method

The elastic energy of a deformable solid is the work done by the elastic forces between the undeformed and deformed positions, integrated across the whole domain. The numerical integration of the elastic forces is classically performed at the tetrahedron level in regular finite element methods. In our approach, we partition the domain Ω into M integration regions V^m consisting of a set of tetrahedra. In the spirit of our affine frame control nodes, we use a high order integration rule called elastons introduced in [4] and generalized in [2]. The classical integration approach assumes a constant force within each integration region V^m. The elaston framework relies on a first order Taylor expansion of the field to be integrated in order to reach a higher level of accuracy. More precisely, a field $f(x)$ is locally approximated as $f(x) \approx \mathbf{F}\,\tilde{p}$ where $\mathbf{F}$ is a vector containing the value of the field and its derivatives at the center of V^m, and $\tilde{p}$ is the polynomial basis of order α in dimension d, for example $[1, x, y, z]$ at order 1, in 3D. Finally, the integration is performed as :

$$\int_\Omega f(x)\ dx = \sum_m \int_{V^m} f(x_m)\ dx = \sum_m \mathbf{F}_m \int_{V^m} \tilde{p}\ dx$$

In our approach, the strain and stress are approximated by a first order polynomial function in the vicinity of each integration sample which is estimated thanks to a Generalized Moving Least Square (GMLS) interpolation scheme [4].

4 Kinematic Mappings

The mappings are templated functions allowing to project forces, displacement and their derivatives between the affine frame DOFs and the tetrahedral mesh. We present the well known linear blend skinning and the GMLS mapping, very suitable with our first order framework.

4.1 Position and Force Mappings

The mesh vertices are displaced based on a linear blending of the affine frame DOFs using the shape functions defined in section 2.

Let $\bar{x}_j$ be the rest position of the j^{th} mesh vertex. Its deformed position x_j is computed as a function of the affine transformations $\mathbf{T}_i$:

$$\forall j \in [\![1, N]\!],\ x_j = \sum_{i=1}^{n} \phi_i(\bar{x}_j)\mathbf{T}_i \begin{bmatrix} \bar{x}_j \\ 1 \end{bmatrix}$$

Conversely, to compute the resulting force F_i applied to the i^{th} frame DOF, we gather all the forces f_j applied to the vertices with the weighted sum:

$$\forall i \in [\![1, n]\!],\ F_i = \sum_{j=1}^{N} \phi_i\left(\bar{x}_j\right) f_j$$

4.2 GMLS mapping

The GMLS method was shown [4, 1] to be an efficient method to approximate globally a function from sparse discrete values with a minimisation problem. This problem seeks new shape functions $N_i(x)$ representing accurately the function over the whole domain.

$$\mathbf{T}(x) = \sum_{i=1}^{n} \mathbf{T}_i N_i(x)$$

In our framework, this mapping is used to compute the deformation gradients from vertices position at integration points. See [4] for an analytical formulation of $N_i(x)$.

5 Results

The proposed method was tested on different geometries, increasing in complexity. The simulation is performed on an Intel(R) Core(TM) i7-8650U CPU @ 1.90GHz laptop, using the SOFA framework. The method widely uses the Flexible plugin approach of Fig. 2.

5.1 Cube under simple compression

First, we simulate the compression of a cube $[0, 1]^3\ m$ discretized with 420 points and 1402 tetrahedra. Forces of $2000N$ are applied to the bottom and upper faces while other faces are free. The Young modulus is $E = 15MPa$ and Poisson ratio $\nu = 0.49$.

At each simulation, regions are randomly generated by picking seeds among the tetrahedra, then extended according to a classic Voronoï sampling followed by a Lloyd relaxation.

The integration samples are generated with the same process within the regions. Their number is proportional to the volume of the zone. To evaluate the simulation results, we use a full order finite element model referred as FEM in which the control nodes are placed at the mesh vertices and the DOFs are the

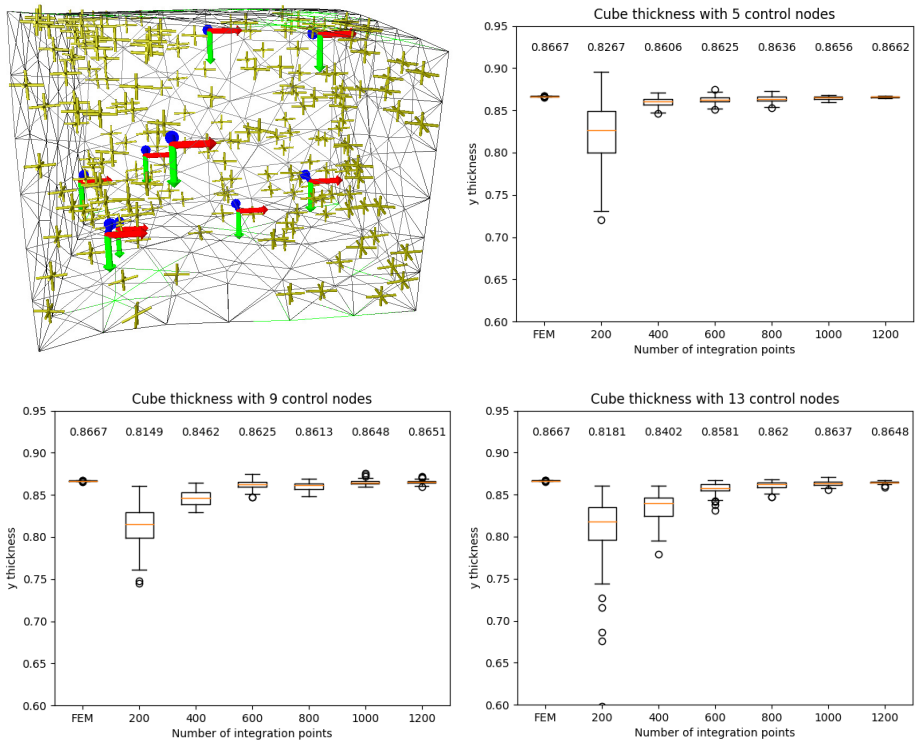

Fig. 4. Thickness of the cube under compression. Top left figure corresponds to the deformed cube with 9 regions and 200 integration points. The yellow crosses represent the deformation gradients at these points. Frames indicate the position of the control nodes.

3 components of the displacement vector. Barycentric shape functions are used within the elements and the integration is performed within the tetrahedra.

Table 1 shows the computation time increasing accordingly to the number of affine control nodes and integration points (from 0.088 to 2.669 seconds). Choosing suitable numbers of DOFs and integration points will consist in a trade off between speed and accuracy, depending on the complexity of the deformation to approximate. By selecting as many integration points as the number of tetrahedra, the simulation time of the proposed method is similar to the FEM's.

The thickness of the cube under compression is studied for one, five and nine control nodes. The relative error compared to FEM is listed in Table 1. The compression, consisting in a simple scaling, is exactly represented by one affine transformation. In this case, one integration sample is sufficient to represent the deformation. The results for one region validate the simulation in this sense but are not physically interesting. The other experiments show that a denser sampling will lead to a more accurate solution. This is expected since the deformations are captured in more local areas.

Gauss Points / Zones		1	5	9
200	Time (s)	0.088	0.575	1.157
	Error (%)	0.0	3.796 ± 9.864	4.511 ± 4.469
500	Time (s)	0.116	0.891	1.823
	Error (%)	0.0	1.142 ± 1.297	2.192 ± 3.987
800	Time (s)	0.144	1.125	2.263
	Error (%)	0.0	0.312 ± 1.228	0.646 ± 1.608
1100	Time (s)	0.173	1.409	2.669
	Error (%)	0.0	0.104 ± 1.203	0.115 ± 1.064
1400	Time (s)	0.204	1.293	2.402
	Error (%)	0.0	0.081 ± 0.272	0.081 ± 0.380

Table 1. Cube computation time and relative error comparison. The error uncertainty represents the tilting of the upper and bottom faces. FEM computation time is 2.41s.

Since the regions are randomly generated, their size and position can vary, leading to areas less represented in integration points. We observed that the stiffness is higher in the well sampled areas. Such a heterogeneity causes the upper and bottom faces to tilt. This phenomena can be observed for a high number of regions and low number of integration points, corresponding to a high uncertainty in Table 1. For example, the top left figure in Fig. 4 shows the random sampling of integration points. At the bottom of the cube, the lack in integration points introduces errors in the deformations leading to the bending of the cube's edge.

5.2 Inflation of a truncated ellipsoid

The second experiment deals with Dirichlet boundary conditions on an axially symmetric shape. We study the deformations of a truncated ellipsoid discretized with 1801 points and 6181 tetrahedra. The regions are linearly generated. One fixed-size region is placed at the apex. A pressure force of $1000N$ is applied on the interior triangles along the normal surface. The following results are obtained with 4000 integration points, $E = 1GPa$ and $\nu = 0.49$.

The top mesh vertices are fixed with a projective constraint. To do so, we modify the control node location and shape function of all regions sharing at least one mesh vertex with the boundary. For these regions, the affine control node is arbitrary placed on the boundary. The shape function is equal to 1 on the boundary vertices and then classically decreases on the remaining vertices. We finally project the constraint on the previously selected DOFs, thus constraining the mesh vertices on the boundary.

The orange curve on Fig. 5 represents the converged FEM deformation. Our method tends to converge toward the FEM one while increasing the number of control nodes. These results are two to three times faster than the full order method.

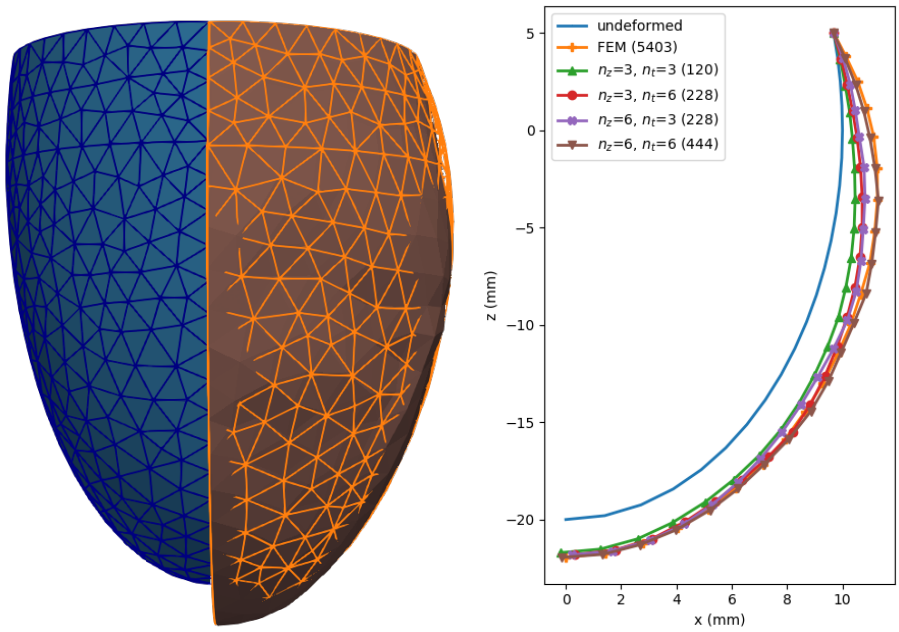

Fig. 5. Left: ellipsoid at rest (blue with edges) and deformed with full (orange wireframe) and reduced (plain brown) models. Right: position of the points on the external surface in the plane $(x^+, 0, z)$. n_z corresponds to the number of zones on the vertical axis and n_t along the circumference of the ellipsoid (plus one zone for the apex). The number of DOFs of each model is indicated in parenthesis.

6 Discussion

On the ellipsoid case, we can notice that the external surface position is directly dependent on the number of regions. Considering the circular shape of the ellipsoid, tangential forces in large regions cancel each other resulting in a lower pressure force mapped to the control node. This effect tends to minimize the inflation for small number of regions.

Furthermore, it is good to notice that with the projective constraint, the slope of the curve near the Dirichlet boundary condition is well approximated. Another solution is to apply very stiff forces on the top nodes as boundary condition. However, this leads to stiffer top regions. In this case, the forces are mapped to the control nodes, thus influencing other vertices contained in these regions. This problem does not appear in the classical FEM since the shape functions are defined at the element level. With the projective constraint applied to the control nodes on the boundary and smoothly decreasing shape functions, this problem is tackled.

Finally, we observed small bumps on the deformed mesh, more visible for a large number of regions and probably due to the shape functions definition. The

inflation seems more pronounced at the center of the regions than the reference one as it is visible on the ellipsoid Fig. 5. This phenomena is reduced when a, the parameter of the sigmoid shape function, is high but leads to a smaller deformation.

7 Conclusion

The method presented in this paper shows promising advances in reducing the computation time and number of integration samples. Deformations on simple geometries are well approached with suitable parameters and validate the method. More complex geometries, such as the truncated ellipsoid, which is a simplified model of a ventricle, are also well approached by poly-affine deformations providing a sufficient number of DOFs. To be efficient, this hybrid method still requires a fine mesh for the offline computation of the geodesic distance as well as the regions volume. With circular shapes, the required number of control nodes to obtain an accurate solution is still high to efficiently use the large regions defined by the AHA segments. Moreover, further work needs to be done to understand the bumps issue. Finally, simple boundary conditions are well handled providing an extra care on the control nodes location and the mapping between the mesh vertices and the basis of affine degrees of freedom.

References

1. Fries, T.P., Matthies, H.G.: Classification and overview of meshfree methods. Informatik-Berichte der Technischen Universität Braunschweig **2003-03** (2004)
2. Gilles, B., Faure, F., Bousquet, G., Pai, D.K.: Frame-based interactive simulation of complex deformable objects. In: Deformation Models. LNCVB, Springer (2013)
3. Lluch, E., De Craene, M., Bijnens, B., Sermesant, M., Noailly, J., Camara, O., Morales, H.: Breaking the state of the heart: meshless model for cardiac mechanics. Biomechanics and Modeling in Mechanobiology (06 2019)
4. Martin, S., Kaufmann, P., Botsch, M., Grinspun, E., Gross, M.: Unified simulation of elastic rods, shells, and solids. ACM Trans. on Graphics (Proc. SIGGRAPH) **29**(3), 39:1–39:10 (2010)
5. Mcleod, K., Sermesant, M., Beerbaum, P., Pennec, X.: Spatio-Temporal Tensor Decomposition of a Polyaffine Motion Model for a Better Analysis of Pathological Left Ventricular Dynamics. IEEE Trans. on Medical Imaging **34**(7), 1562–1675 (2015)
6. Pernod, E., Sermesant, M., Konukoglu, E., Relan, J., Delingette, H., Ayache, N.: A multi-front eikonal model of cardiac electrophysiology for interactive simulation of radio-frequency ablation. Computers and Graphics **35**, 431–440 (2011)
7. Zhou, Y., Bernard, O., Saloux, E., Manrique, A., Allain, P., Makram-Ebeid, S., Craene, M.D.: 3D harmonic phase tracking with anatomical regularization. Medical Image Analysis **26**(1), 70 – 81 (2015)